Journal of Non-Crystalline Solids 444 (2016) 43–48

Contents lists available at ScienceDirect

Journal of Non-Crystalline Solids

journal homepage: www.elsevier.com/locate/jnoncrysol

Plasma-enhanced atomic layer deposition of zinc phosphate

T. Dobbelaere [a,*], M. Minjauw [a], T. Ahmad [a], P.M. Vereecken [b], C. Detavernier [a,*]

[a] Department of Solid State Sciences, Ghent University, Krijgslaan 281 S1, 9000 Gent, Belgium
[b] imec, Kapeldreef 75, 3001 Leuven, Belgium

ARTICLE INFO

Article history:
Received 22 February 2016
Received in revised form 7 April 2016
Accepted 15 April 2016
Available online 8 May 2016

Keywords:
Atomic layer deposition
Plasma-enhanced
Phosphates
Zinc phosphate

ABSTRACT

Zinc phosphate thin films were grown by plasma-enhanced atomic layer deposition (ALD) using a sequence of trimethyl phosphate (TMP, Me_3PO_4) plasma, O_2 plasma, and diethylzinc (DEZn, Et_2Zn) exposures. The film growth was monitored by in-situ spectroscopic ellipsometry. At a substrate temperature of 300 °C, linear and saturated growth was observed with a remarkably high growth rate of 0.92 nm/cycle. As-deposited films were smooth, amorphous and very hygroscopic, suggesting a phosphorus-rich composition resembling zinc phosphate glass. Upon annealing in air, crystalline zinc phosphate and pyrophosphate phases were formed.

© 2016 Elsevier B.V. All rights reserved.

1. Introduction

1.1. Atomic layer deposition

Atomic layer deposition (ALD) is a thin film deposition technique in which material is grown in a layer-by-layer fashion by alternating exposures to chemical vapors. In contrast to chemical vapor deposition (CVD), the precursors are introduced separately, with pumping or purging steps in between. This causes self-limiting reactions to take place on the substrate surface, resulting in slow but precisely controlled film growth. Many ALD processes exist for oxides, ii-vi and iii-v semiconductors, metal nitrides, metals, metal sulfides, and fluorides [1]. ALD of phosphates has been reported for aluminium phosphate [2–7], calcium phosphate [8], titanium phosphate [4,9], lanthanum phosphate [10], lithium phosphate [11,12], iron phosphate [13,14], and lithium iron phosphate [15]. The phosphorus precursor is almost always trimethyl phosphate (TMP) because it is a stable liquid with a suitable vapor pressure. Its high stability, however, also limits its use as an ALD reactant, often resulting in very slow growth or difficulty in incorporating sufficient amounts of phosphorus into the film.

We previously reported a novel plasma-enhanced atomic layer deposition (PE-ALD) process for aluminium phosphate, which was based on the use of a TMP plasma instead of vapor [7]. By studying the reaction mechanism using in-situ techniques, we concluded that the combined action of TMP plasma with O_2 plasma created phosphoric acid-like precursor species on the substrate surface, which subsequently reacted with trimethylaluminium (TMA) to produce aluminium phosphate. We further hypothesized that the same process could be used to grow other phosphates by swapping TMA with a different metal precursor. In this work, diethylzinc (DEZn) was used as the metal precursor, and this resulted in the plasma-enhanced atomic layer deposition of zinc phosphate.

1.2. Zinc phosphate

ALD growth of zinc oxide is a well-known process that is typically achieved by combining diethylzinc with a reactant such as water vapor [16,17], ozone [18,19] or oxygen plasma [20,21]. Phosphorus has been incorporated into ALD-grown ZnO as a p-type dopant [22,23] in concentrations below 5 at.% and in the crystalline form (wurtzite structure). To the best of our knowledge, ALD of amorphous zinc phosphate has not been previously reported. Amorphous (or "glassy") zinc phosphate is, however, an interesting material with applications in photonics (including femtosecond laser waveguide writing [24] and hosting luminescent ions [25]), in glass-metal sealing, and in glass-polymer composites [26]. Its glass properties can be tuned by adding e.g. aluminium oxide and varying the Al/Zn and/or P/O ratios [27], for which ALD could be a very suitable technique.

2. Experimental

2.1. Deposition system

Depositions were carried out in a home-built pump-type PE-ALD reactor, shown schematically in Fig. 1. All parts were stainless steel, unless otherwise specified.

The deposition chamber was continuously evacuated by a turbomolecular pump to a base pressure of approx. 4×10^{-6} mbar.

* Corresponding authors.
E-mail addresses: thomas.dobbelaere@ugent.be (T. Dobbelaere), christophe.detavernier@ugent.be (C. Detavernier).

http://dx.doi.org/10.1016/j.jnoncrysol.2016.04.032
0022-3093/© 2016 Elsevier B.V. All rights reserved.

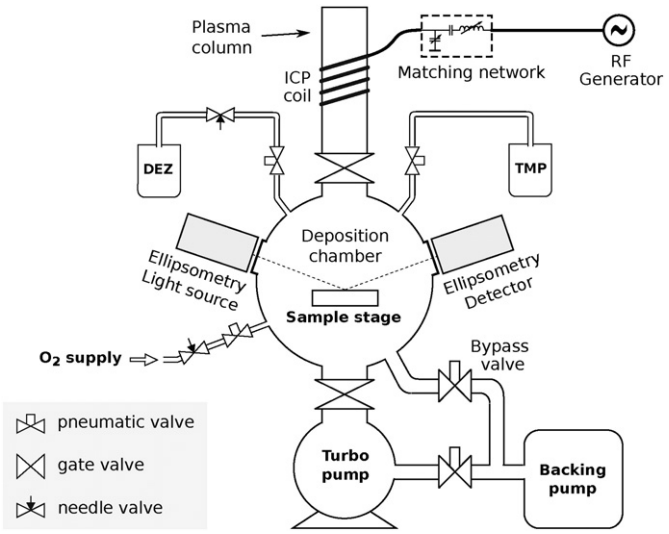

Fig. 1. Schematic drawing of the deposition system used in this work, showing the vacuum chamber, precursor connections, and the plasma system.

Precursor vapors and gases were admitted through computer-controlled pneumatic valves. The TMP precursor (Sigma-Aldrich, 97%) was heated to 45 °C. The DEZn precursor (Sigma-Aldrich) was used at room temperature, and its flow was regulated by a needle valve. The flows of DEZn and O_2 were adjusted to reach a pressure of 5×10^{-3} mbar in the deposition chamber. The temperature of the chamber walls was set to 100 °C, and all precursor tubes leading to the chamber were additionally heated to prevent any precursor condensation. On top of the chamber, a gate valve leads to a fused quartz column wrapped by a copper coil. The coil was connected to a 13.56 MHz RF generator (ENI GHW-12Z) and a matching network in order to generate an inductively coupled plasma in the column. The remote plasma was generated by feeding vapor or gas from the chamber to the plasma column through the gate valve and pulsing the RF generator. The plasma power was set to 200 W for the TMP plasma and 300 W for the O_2 plasma, and the impedance matching was tuned to minimize the reflected power on both. The substrates consisted of p-type silicon (100) wafer pieces and were mounted to a heated copper block with PID temperature control.

2.2. Deposition process

A single cycle of a typical deposition process consisted of: TMP plasma / pumping / O_2 plasma / pumping / DEZn exposure / pumping. All precursors were introduced into the chamber while it was continuously pumped, reaching a partial pressure of 5×10^{-3} mbar in the deposition chamber. In between precursor pulses, pumping times of 20 s were found sufficient to bring residual pressures to below 4×10^{-5} mbar, thereby avoiding CVD side reactions.

2.3. Material characterization

In-situ spectroscopic ellipsometry measurements were performed with a J.A. Woollam M-2000 ellipsometer working in the ultraviolet-visible region and using the CompleteEASE software for fitting and data analysis. The optical model consisted of a silicon substrate covered by a single layer which satisfied a Cauchy dispersion relation. Measurements were acquired after each deposition cycle. Systematic parameters (angle offsets, window corrections) were fitted prior to deposition and then held fixed. The final thickness and the Cauchy parameters were fitted to the measurement acquired after the last cycle (i.e. after deposition). A growth curve was then obtained by fitting the thickness to each measurement, keeping all other parameters fixed.

An FEI Quanta 200 F scanning electron microscope was used for SEM imaging and energy-dispersive X-ray spectroscopy (EDX) analysis, using an electron beam energy of 5 keV. EDX spectra were acquired while scanning over an area of 500 × 500 μm during an acquisition time of 100 s. In-situ XRD during annealing was performed in a home-built setup [28–30]. The annealing atmosphere was ambient air; the XRD patterns were acquired using a Cu Kα X-ray source and a position sensitive detector. X-ray Photoelectron Spectroscopy (XPS) analysis was performed on a Thermo Scientific Theta Probe XPS instrument using Al Kα X-rays generated at 15 kV and 70 W and focused to a spot size of 0.3 mm by an MXR1 monochromator gun. The sample surface was etched by Ar + ions at an acceleration voltage of 3 keV and a current of 2 μA. Atomic Force Microscopy (AFM) was performed using an Omicron VT XA AFM system operating in non-contact mode, with a base pressure of 10^{-10} mbar.

3. Results and discussion

3.1. Hygroscopicity

The deposited zinc phosphate layers were very hygroscopic: upon removal from the deposition system and exposure to ambient air, the thin films gradually changed color, and eventually (in the course of a few days) became non-uniform and irregular in appearance. Furthermore, the film color changed immediately by simply exhaling on it, indicating rapid swelling due to the absorption of moisture. This complicated the analysis of the samples, e.g. making it impossible to measure film thicknesses in a reproducible way by X-ray reflectometry due to uncontrollable humidity exposure which influences the layer thickness and/or density.

As the most common form of zinc phosphate, zinc orthophosphate ($Zn_3(PO_4)_2$), is not hygroscopic [31], the deposited material must have a different composition. Hygroscopicity typically increases with phosphorus content, as the bridging oxygens between phosphorus atoms are highly susceptible to hydrolysis. In the case of zinc ultraphosphate, where the amount of P_2O_5 is bigger than the amount of ZnO, each phosphate group can bond with three other phosphate groups, and the resulting P—O bonds are particularly reactive with water [32]. We can therefore anticipate that the deposited material must be a phosphorus-rich form of zinc phosphate, likely in the metaphosphate to ultraphosphate category.

3.2. Optical model

Due to the difficulty of accurate ex-situ characterization, the deposition process was completely characterized by in-situ spectroscopic ellipsometry, making it possible to measure the layer growth without breaking the vacuum. A well-fitting model of the optical properties of the deposited layer is a necessary requirement for this, and in this case a Cauchy dispersion relation of the form $n(\lambda)=B+C/\lambda^2+D/\lambda^4$ was used. The parameters were determined by least-squares fitting as $B=1.30\pm0.01$; $C=(-0.0085\pm0.0014)$ μm^2; and $D=(0.0013\pm0.0002)$ μm^4. This dispersion relation is plotted in Fig. 2. The same figure also shows the evolution of the measured Psi and Delta angles during different stages of the layer growth, showing good correspondence with the calculated curves based on the aforementioned Cauchy model where the thickness was the only adjusted parameter. The measured refractive index of 1.29 ± 0.01 (defined at a wavelength of 589 nm) is remarkably low; this might be related to the high phosphorus content of the deposited material, due to the low ionic refractivity of phosphorus [33].

Download English Version:

https://daneshyari.com/en/article/1480308

Download Persian Version:

https://daneshyari.com/article/1480308

Daneshyari.com